Colloids and Surfaces A: Physicochemical and Engineering Aspects 622 (2021) 126702

Contents lists available at ScienceDirect

Colloids and Surfaces A: Physicochemical and Engineering Aspects

journal homepage: www.elsevier.com/locate/colsurfa

# Effect of width/height of the gap between piston and wall on the performance of a novel small volume emulsification device

Angeliki P. Chondrou, Thodoris P. Karapantsios, Margaritis Kostoglou *

*Department of Chemical Technology, School of Chemistry, Aristotle University of Thessaloniki, University Box 116, 541 24 Thessaloniki, Greece*

## HIGHLIGHTS

- Emulsification performance assessment of geometric features of oscillating pistons.
- Microscopy images analysis and phase separation observations for identification of the broad droplet size distribution.
- Reducing the gap thickness and increasing the piston thickness improves the emulsification efficiency.

## GRAPHICAL ABSTRACT

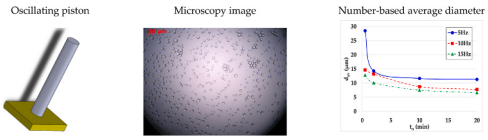


## ARTICLE INFO

*Keywords:*
Oscillating piston
Emulsification device
Small volume
Microscope analysis
Droplet size distribution
Droplets breakage

## ABSTRACT

The concept of a small volume emulsification device developed by the authors is further studied in the present work. Following suggestions of previous work, five different piston plates with orthogonal edges are constructed to oscillate inside a small cube-shaped cell. The different pistons yield several combinations of gap width and height between the plates and the walls of the cell. Their performance is assessed by performing emulsification experiments over an extensive range of piston stroke frequency and emulsification time for a specific non-coalescing system (fixed oil fraction and surfactant concentration). The resulting droplet size distributions are estimated by microscopy images analysis and by phase separation observations. The combined information from these techniques is necessary in order to register the broad size range of droplets. A semiquantitative analysis of the flow field in the gap reveals that droplet breakage process starts at the laminar boundary layers developed between the piston and the cell walls and allows characterization of this field. A theoretical analysis for the mechanism of droplet breakup is presented. The analysis of experimental results demonstrates that four of the five tested piston plates are appropriate for emulsification regarding the generated droplet size distribution and the choice among them requires additional criteria, e.g. energy requirements.

## 1. Introduction

Emulsions dominate our daily life since they are widely used in foods, cosmetics, pharmaceuticals, agricultural products as well as they are applied to petroleum industry and oil recovery processes. They are mixtures of two, partially or completely, immiscible liquids. In an emulsion, the first liquid (dispersed phase) is dispersed inside the second liquid (continuous phase) in the form of droplets [1,2]. Depending on which liquid constitutes the continuous and the dispersed phase there are oil-in-water emulsions (O/W) and water-in-oil emulsions (W/O) [3].

The two phases (liquids) alone, oil and aqueous phase, under agitation create a thermodynamically unstable system because of the large liquid/liquid interfacial energy. Therefore, in order to kinetically stabilize emulsions and achieve long-term emulsion stability, a third

* Corresponding author.
*E-mail address:* kostoglu@chem.auth.gr (M. Kostoglou).

https://doi.org/10.1016/j.colsurfa.2021.126702
Received 10 March 2021; Received in revised form 16 April 2021; Accepted 19 April 2021
Available online 24 April 2021
0927-7757/© 2021 Elsevier B.V. All rights reserved.

component, the emulsifier is needed [4,5]. Surfactants are mainly used as emulsifiers as well as solid particles, proteins and blends of them. A surfactant, composed of a hydrophilic head and a hydrophobic tail, usually soluble in the external continuous phase, is adsorbed at the liquid/liquid interface and a protective layer is formed. Its existence leads to the reduction of interfacial tension and creates a barrier to the coalescence phenomenon [6]. Emulsions stability is found to be strongly dependent on many different factors: (1) the size distribution of the oil droplets, the smaller the size range the more stable the emulsion, (2) the volume ratio of the two phases, the increase of the interfacial film area leads to a more unstable system and (3) the bulk viscosity of the continuous phase [7–9].

Several phenomena contribute to emulsion destabilization during storage. The gravity driven processes of creaming and sedimentation are facilitated by (i) interface driven phenomena of droplets aggregation (flocculation and coalescence) and (ii) Ostwald ripening. The interface driven phenomena lead to the increase of droplet size and finally the system separates into the two initial immiscible bulk liquids (phase segregation) [10]. As mentioned above, emulsion stability is strongly related to the droplet size distribution which can be measured by several techniques, e.g., microscopy, light scattering, diffusing wave spectroscopy, electrical impedance spectroscopy [11–13]. Some of these techniques provide information regarding size distributions based on droplet number while others provide information based on higher order features such as droplet surface area or droplet volume.

Mechanical energy is required to break up droplets into smaller sizes and so lead to an emulsion. Different flow conditions (from laminar to turbulent) are employed for the non-spontaneous emulsification process to take place depending on the method. There is a wide range of emulsification methods: shaking, rotor-stator devices, membranes, microchannels [14], high pressure homogenizers and ultrasound generators [15–18]. To break up a droplet into smaller ones it is necessary the droplet shape to be deformed [19]. This occurs when the system is subjected to forces from the continuous phase.

In our previous study, an innovative miniature pulsating emulsification device has been developed where droplets breakup is accomplished by the periodic up and down movement of a rectangular plate, fixed at the tip of a piston, inside a cube-shaped cell triggered by a stepper motor [20]. The device resembles FOAM-C, a European Space Agency instrument designed and constructed for experiments in the International Space Station (ISS). The laboratory breadboard is used on-ground for testing different experimental conditions to select a proper range of experimental parameters for the ISS experiments and to gather sufficient evidence for the interpretation of the results. The device offers the advantage of using only small quantities of liquids and surfactants since the experimental cell volume does not exceed 4 mL. This makes the device particularly suitable for testing rare or expensive cosmetics or medicines. Moreover, the rectangular cell with flat walls allows direct optical observation, which is a severe limitation of cylindrical-shaped rotor-stator devices. The use of microfluidic devices for emulsification (e.g. impingement of two streams [21]) has similar features to the present device (e.g. allows optical observations [22] and produces a small volume of emulsion starting from separated liquids). However, there are also distinct differences with respect to the present device (e.g. continuous vs batch operation, need for high pressures).

Taking into consideration the results of the previous work [20], the

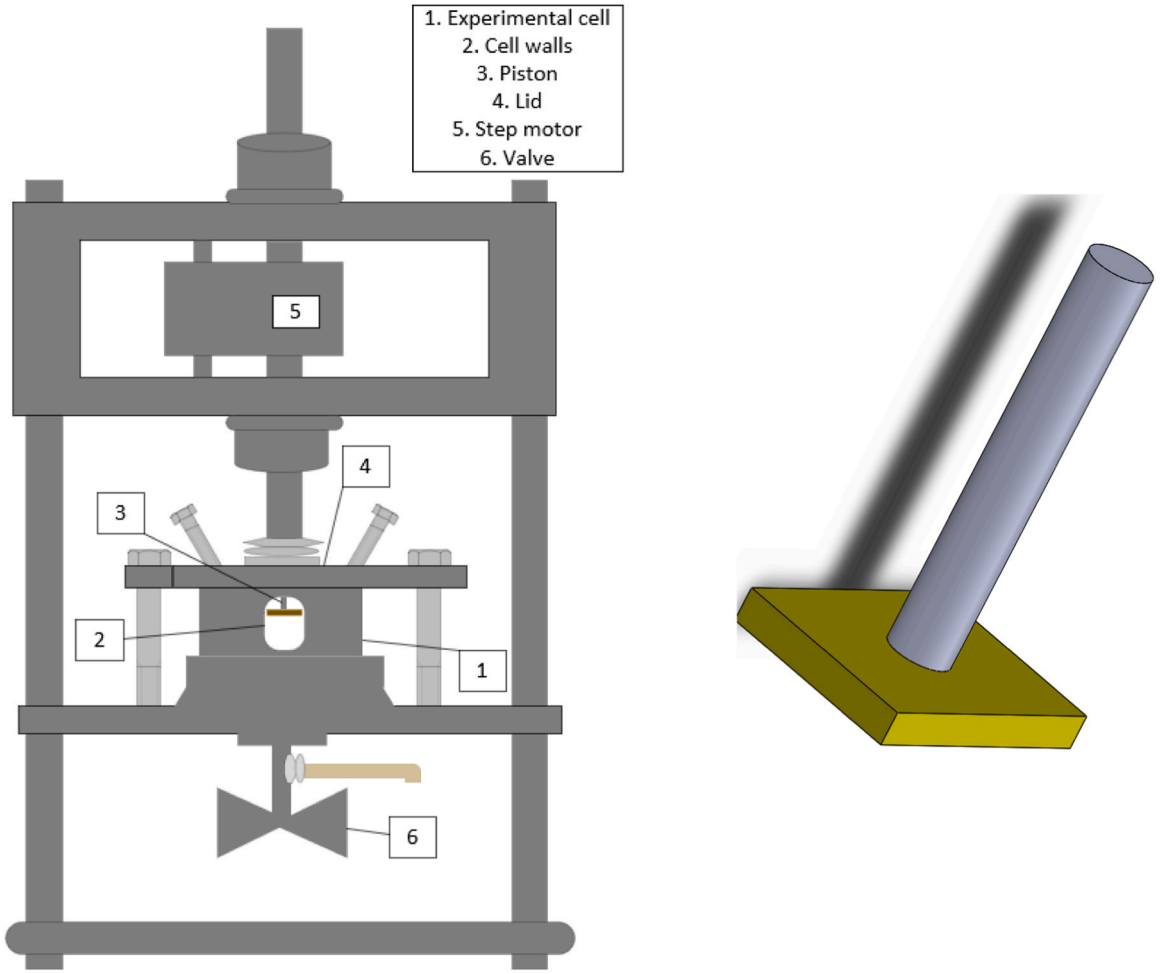


**Fig. 1.** Schematic representation of the emulsification device and of the piston with the orthogonal plate at its tip.

aim of the present study is to test five different piston plate geometries, dictating different width and height of the gap between the plate and the cell walls, regarding the ensuing droplets size distribution and, consequently, emulsion stability. Evaluation of the stability of the produced emulsions is investigated by optical means and droplets size distributions are discussed with emphasis on their dependence from the examined experimental parameters (pulsation stroke frequency and emulsification duration). Finally, the flow field in the gap is discussed regarding its role for droplets breakup.

## 2. Materials & methods

The emulsification process takes place at a miniature pulsating emulsification device. The whole device is made of aluminum and its dimensions are 200 × 300 × 400 mm. The core of the device is a rectangular experimental cell (12 × 14 × 26 mm) with four glass side walls of 1 mm thickness. In addition, a valve is connected to the bottom of the experimental cell with a plastic tube on it. The glass side walls offer four ports for optical recordings and lighting. Incorporated to the cell's lid is a piston which consists of a cylindrical rod with a thin aluminum plate of uniform height attached to its tip. The schematic representation of both the emulsification device and the piston are presented in Fig. 1. The total useful (occupied by liquids) volume of the experimental cell depends on the employing piston every time, however, it does not exceed 4 mL. The piston moves periodically up and down and its route is always 11 mm. Although the height of the cell is 26 mm the piston route is only 11 mm because the lid occupies a part of the cell volume. Immediately after the end of the emulsification process the bottom valve allows collecting the produced emulsion for optical observation and microscopy analysis. Five pistons are constructed which differ in the length or in the height of their plate sides. These features dictate different width and height of the gap between the plate and the cell walls. The plate (i.e., gap) dimensions have a crucial effect on the droplet size distribution of the produced emulsions. Piston's characteristics are presented in Table 1. The piston is driven by a stepper motor (Model: 23HS9430, Company: Longs Motor). A rack-pinion gear is used to convert the rotary motion of the stepper motor into the linear motion of the piston. A custom made software (Mach3) is used to control the stepper motor. The two parameters controlled by the software are stroke frequency (f) and total pulsation duration ($t_n$). Due to mechanical constraints the maximum stroke frequency is 20 Hz whereas there are no limitations regarding the pulsation duration.

The main working materials for the preparation of oil in water emulsions are Millipore water and Dodecane (Sigma-Aldrich). The density and viscosity of Millipore water are 0.997 g/cm$^3$ and 0.89 mPa s, respectively. Dodecane is a hydrocarbon in the form of a colourless liquid. The density and viscosity of dodecane are 0.75 g/cm$^3$ and 1.34 mPa s, respectively. In all experiments, the water soluble anionic surfactant, Sodium Dodecyl Sulfate (SDS; Sigma-Aldrich) with purity ≥ 98.5%, is used as emulsifier. SDS is an odorless surfactant in the form of a white powder and its critical micellar concentration (CMC) is 2.5 g/L [23]. SDS has been extensively studied and it is an excellent detergent, emulsifier and food additive.

An aqueous solution of SDS constitutes the aqueous phase and dodecane the organic phase in the preparation of emulsions. In the present tests, the surfactant concentration is 1 CMC and the oil volume fraction φ is 10%. In our previous work [20] the effect of surfactant concentration on the emulsification efficiency in the device was examined. Here the concentration of 1 CMC is selected as it is large enough to prevent coalescence and small enough to alter the viscosity of the dispersion. The use of similar amounts of surfactant to stabilize emulsions has been recorder in literature [24]. Since the lid of the cell (with the integrated piston) is already in place, the insertion of liquids is done through two small tubes which work as communication ports between the cell interior and the surroundings. The aqueous phase is added first to the experimental cell and dodecane (organic phase) follows. Before the onset of pulsation both ports are tapped with vanes and the cell interior is isolated.

Immediately after the end of pulsation the bottom valve of the experimental cell is opened to collect the produced emulsion. At this instant the emulsion is fully homogeneous. A sample of approximately 0.2 mL is then diluted into a glass tube which contains a 5% SDS solution to inhibit droplets coalescence. The primary emulsion is then mildly hand shaken and visual observations are employed to determine the instantaneous heights of both the creamy and aqueous phase in the tube. In fact, at short times after decanting the aqueous phase constitutes also an emulsion, like the creamy phase, but with a much smaller oil proportion. Photographs are taken with a camera (Canon EOS-350D) at different time intervals for some hours. The setting is made so that the camera takes automatically one picture every 5 s for the first 10 min and then one picture every 60 s until the end of observation. The distance of the camera and the glass tube is 40 cm in order that several tubes can be photographed from the camera at the same time. Analysis of the obtained pictures allows calculation of the average phase separation front velocity, $U_b$. The equation used is:

$$U_b = \frac{h_{end} - h_0}{t_{end}} \quad (mm/s) \tag{1}$$

where, $h_{end}$ is the height of the aqueous phase at the end of separation (mm), $h_0$ is the height of the aqueous phase right after decanting (mm), $t_{end}$ is the time where the separation reaches a steady plateau.

In parallel, a sample is taken from the diluted emulsion in the 5% SDS solution and is placed on a microscope slide. After a cover glass is placed above the sample, a Zeiss, Axiostar Plus microscope combined with a Canon Powershot A640 video camera is used to take high resolution (10 megapixels) images of oil droplets in the sample. In this study, the employed total microscope magnification is x100. This technique provides information regarding the number-based droplet diameter and the smallest droplet that can be measured is 0.7 μm. Ten microscopy images of each emulsion are analyzed with BubbleSEdit, a custom made software for bubbles/droplets detection [25]. The software can be operated

**Table 1**
Plate (of the piston) and gap (between plate and cell walls) characteristics.

| | Height (mm) | Gap between the plate and the cell walls (mm) | Gap between the plate and the top part of the cell (mm) | Gap between the plate and the bottom part of the cell (mm) |
|---|---|---|---|---|
| **1** | 1.62 | 0.66 | 2.33 | 2.38 |
| **2** | 1.62 | 0.4 | 2.33 | 2.38 |
| **3** | 1.62 | 0.25 | 2.33 | 2.38 |
| **4** | 1 | 0.25 | 1.45 | 1.5 |
| **5** | 2.5 | 0.25 | 2.95 | 3 |

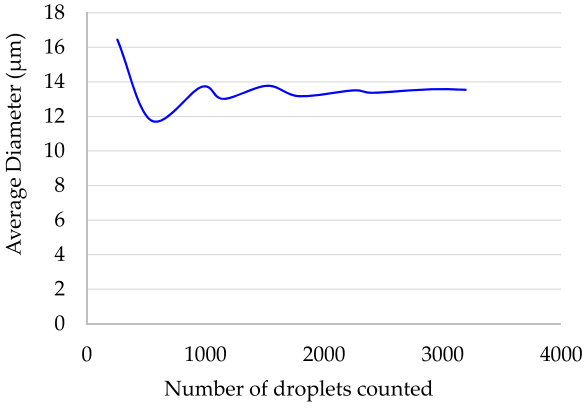


**Fig. 2.** Convergence of the average droplet diameter as the number of considered droplet increases.

**Table 2**
Experimental values of the stroke frequency and the emulsification time in the present experiments.

| | Experimental Parameters | |
|---|---|---|
| | f (Hz) | $t_n$ (min) |
| **1** | 5 | 0.5 |
| **2** | 5 | 2 |
| **3** | 5 | 10 |
| **4** | 5 | 20 |
| **5** | 10 | 0.25 |
| **6** | 10 | 0.5 |
| **7** | 10 | 2 |
| **8** | 10 | 5 |
| **9** | 10 | 10 |
| **10** | 10 | 20 |
| **11** | 15 | 0.25 |
| **12** | 15 | 0.5 |
| **13** | 15 | 2 |
| **14** | 15 | 5 |
| **15** | 15 | 10 |
| **16** | 15 | 20 |
| **17** | 20 | 0.25 |
| **18** | 20 | 2 |
| **19** | 20 | 5 |
| **20** | 20 | 10 |

either manually or automatically. Each image has a different number of droplets. However, in each of the produced emulsions more than 3.000 droplets are analyzed. A typical case of convergence of the average droplet diameter as the number of considered droplet increases is depicted in Fig. 2.

Experiments are conducted using all five Pistons. Two are the necessary experimental parameters to completely characterize the pulsating emulsification device: 1) stroke frequency (f) and 2) emulsification duration ($t_n$). Four different stroke frequencies are applied during the experiments (5, 10, 15, and 20 Hz) whereas the emulsification duration ranges from 15 s to 20 min. The experimental conditions are summarized in Table 2. Test experiments are performed and the temperature of the dispersion at the end of emulsification is measured to check that there are no measurable viscous heating effects even for the largest employed values of f and $t_n$.

## 3. Experimental results

All examined emulsions gradually destabilize and this is reflected in the time required for the complete water phase separation's ($t_{end}$). The lower the $t_{end}$ the less stable the emulsion. As already mentioned, both phases (creamy and aqueous) are actually emulsions but with very different oil proportions. It must be noted that when mentioning water phase separation, this refers to the separation between the creamy phase (high oil volume fraction) and the aqueous phase (low oil volume fraction). Therefore, the interface separating the two phases is not sharp, indicative of a broad droplet size distribution and not of a monodisperse system. At the top of the liquid in the glass tube no continuous layer of oil is observed (even after days) for all the examined emulsions and so it is assumed that coalescence between oil droplets is absent. The combination of emulsion's droplets size and number determines how fast the aqueous phase separates from the creamy one. An emulsion with smaller droplets (more stable) separates slower than an emulsion with larger droplets (less stable). The average phase separation front velocity for all the examined emulsions is presented in Table 3. In the cases where phase separation is almost completed at t = 0 the calculation is not possible. This happens when the droplets' size is too large and it is indicated in the table. Typical images processed to estimate droplet size probability density functions and average diameters appear in Fig. 3.

**Table 3**
Average phase separation front velocities.

| | | | $U_b$ (mm/s) | | | | |
|---|---|---|---|---|---|---|---|
| | f (Hz) | $t_n$ (min) | Piston 1 | Piston 2 | Piston 3 | Piston 4 | Piston 5 |
| **1** | 5 | 0.5 | – | [a] | [a] | [a] | [a] |
| **2** | 5 | 2 | [a] | [a] | 1.04 | 1.06 | 0.88 |
| **3** | 5 | 10 | [a] | [a] | 0.73 | 0.70 | 0.53 |
| **4** | 5 | 20 | [a] | 0.61 | 0.47 | – | 0.36 |
| **5** | 10 | 0.25 | 0.62 | – | – | – | – |
| **6** | 10 | 0.5 | 0.30 | 0.63 | 0.34 | 0.44 | 0.50 |
| **7** | 10 | 2 | 0.5 | 0.48 | 0.22 | 0.27 | 0.39 |
| **8** | 10 | 5 | – | 0.12 | – | – | – |
| **9** | 10 | 10 | 0.43 | 0.12 | 0.15 | 0.16 | 0.14 |
| **10** | 10 | 20 | – | 0.07 | 0.09 | 0.12 | 0.07 |
| **11** | 15 | 0.25 | 0.30 | – | – | – | – |
| **12** | 15 | 0.5 | – | 0.24 | 0.22 | 0.16 | 0.13 |
| **13** | 15 | 2 | 0.19 | – | 0.13 | 0.07 | 0.09 |
| **14** | 15 | 5 | – | 0.12 | – | – | – |
| **15** | 15 | 10 | 0.14 | – | 0.10 | 0.04 | 0.04 |
| **16** | 15 | 20 | – | 0.10 | 0.08 | 0.03 | 0.03 |
| **17** | 20 | 0.25 | 0.15 | – | – | – | – |
| **18** | 20 | 2 | 0.11 | – | – | – | – |
| **19** | 20 | 5 | 0.07 | – | – | – | – |
| **20** | 20 | 10 | 0.06 | – | – | – | – |

-: these conditions have not been examined with the respective Piston
[a] the droplets' size is too large and the calculation is not possible.

First, indicative results of a repeatability check are presented in Fig. 4. The size of oil droplets ranges from ~0.7 to ~70 μm in both repetitions. The number average diameter is 12.2 μm and 12.4 μm for the first and second repetition, respectively. As far as the phase separation front velocity is concerned, it is 4.15 mm/s for the 1st repetition and 4.20 mm/s for the 2nd repetition. Taking the above into consideration, there is a correspondence between repeatability of phase separation front velocity and repeatability of droplet size distributions. In general, the repeatability is considered satisfactory. Several experiments made showed that the uncertainty of $d_{av}$ is less than 1 μm. This values could be used to add error bars in the following figures.

The comparison between the number-based droplet average diameters based on image analysis follows. Four different stroke frequencies (5, 10, 15 and 20 Hz) and six different emulsification times (0.25, 0.5, 2, 5, 10 and 20 s) are employed and the results are presented in Fig. 5. It is generally expected the number average diameter to decrease as either the emulsification time increases (at constant stroke frequency) or the stroke frequency increases (at constant emulsification time). This trend, however, is not always seen in Fig. 5 and there are a few exceptions here and there. For instance, for Piston 1 (Fig. 5(a)) in the case of f= 5 Hz although the number average diameter decreases, as expected, between emulsification times of 2 and 10 min then it unexpectedly increases from 10 to 20 min. Interestingly, there are no such exceptions when looking at Table 3 where the estimated average phase separation front velocity always appears to decrease when either the stroke frequency or the emulsification time increases. The deviation between results of image analysis and results of average phase separation front velocity for some set of parameters will be explained in the discussion section. It is also worth to mention here that, with almost no exception, the number average diameter decreases faster between lower emulsification times (from 0.5 to 2 min) than between higher emulsification times (from 10 to 20 min).

The effect of emulsification parameters (stroke frequency and emulsification time) on droplet size distribution is presented next.

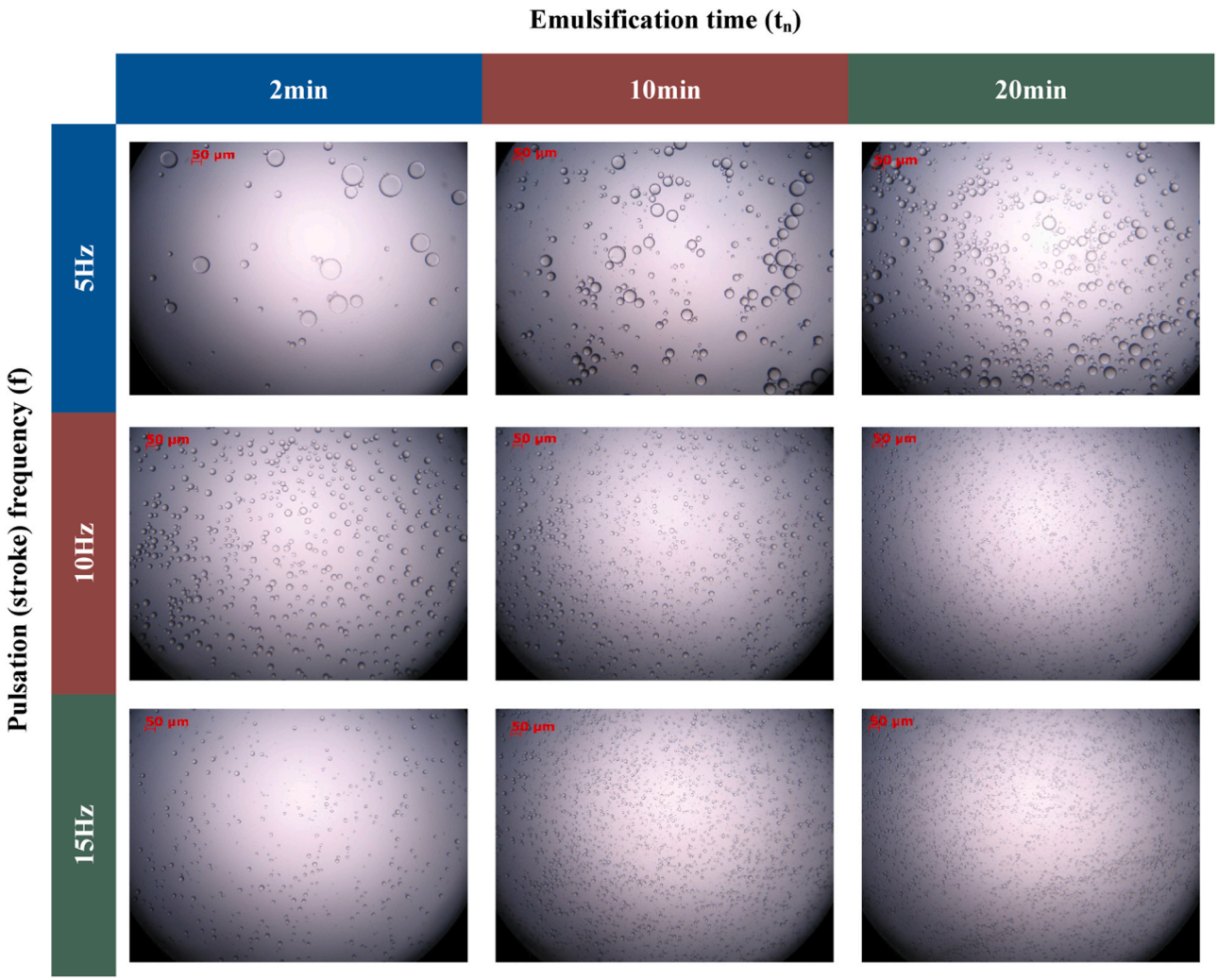


**Fig. 3.** Indicative droplet images at different emulsification times and pulsation stroke frequencies.

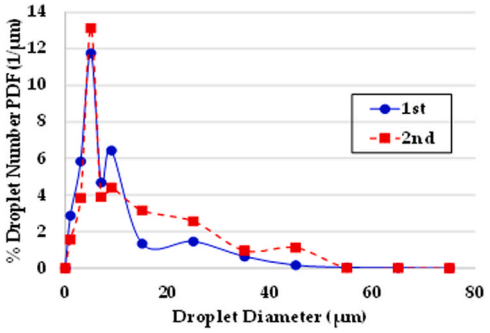


**Fig. 4.** Repeatability test for droplet size distribution.

Indicative results regarding Piston 4 are displayed in Fig. 6. In the examined range of values, as the stroke frequency increases the droplet size distribution becomes narrower (and accordingly more peaked) towards smaller sizes and thus the produced emulsions are more stable.

In the following, experimental results regarding the emulsification time effect on droplet size distribution of the produced emulsions are presented. Indicative results are shown in Fig. 7 for different pistons and stroke frequencies. As the emulsification time increases the droplet size distribution becomes narrower (and accordingly more peaked) towards smaller sizes which means that the produced emulsions are more stable. The effect on the peak of the distributions is seen chiefly when comparing higher values of the emulsification time because at low values peakedness is not so different.

## 4. Problem analysis

### 4.1. Flow field characterization

Droplets deformation and breakage in an emulsion is controlled by the forces generated by the flow of the continuous phase. For this, it is important to analyze the flow field at different regions inside the emulsification cell.

The theoretical analysis of the flow field in the gap has been performed in a previous work [20] in the limit of ignoring flow inertia and acceleration. The focus in that work was on the effect of the non-uniform height of piston plates which introduced complications and rendered the problem 3-dimensional. Here the piston plates have uniform height, δ, along their sides (Fig. 8). This means that (since the transverse aspect ratio $(a_1 + a_2)/w$ of the gap cross section is much larger than one) the flow in the gap can be assumed 2-dimensional, permitting a more thorough analysis of the corresponding flow field.

Let us first discuss the flow field in the regions at the front and rear of the piston as it moves. The time for the piston motion between the two end points of its trajectory is 1/(2 f). During this time, the vorticity produced by the walls penetrate into the fluid at a distance $(\nu/(2\,f))^{0.5}$. This distance is less than 0.35 mm in the present experiments, much

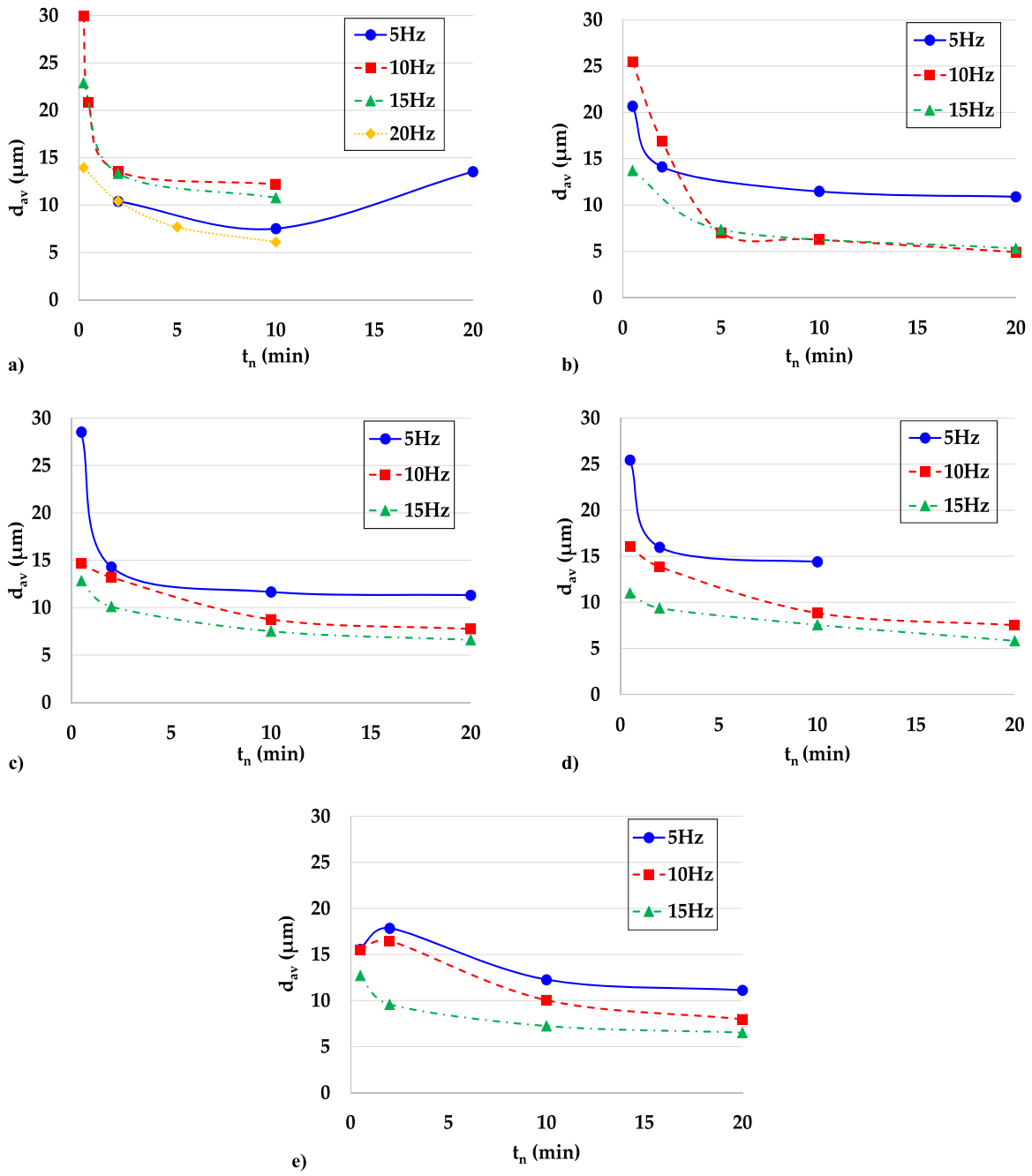


**Fig. 5.** Number based droplet average diameter $d_{av}$ versus emulsification time for different stroke frequencies. a) Piston 1; b) Piston 2; c) Piston 3; d) Piston 4; e) Piston 5.

smaller than $a_1 = 14$ mm and $a_2 = 12$ mm, implying that the wall shear has little effect on flow structure in these regions. The flow in the region in front of the piston can be approximated as irrotational mainly determined by the incompressibility requirement [26]. On the other hand, the flow in the rear region is described by a (one-sided) free shear layer which is restricted by an obstacle [27]. The reduced pressure appearing at the back of the plate creates a wake which induces a dispersion of vorticity of the flow stream ejected from the gap. It can be assumed (this is only an approximation for regions adjacent to the gap) that the velocities in these regions are much smaller than those in the gap. This means that the main region of interest in the present emulsification cell is the flow field in the gap between the plate of the piston and the walls of the cell.

In order to facilitate the analysis, a coordinate system moving with the piston is considered as shown in Fig. 8. A single mass balance for the liquid (by considering the volume evolution of the two domains at the front and rear of the plate and the liquid incompressibility) reveals that the average velocity at the gap entrance will be $U = (a_1a_2/(a_1a_2-(a_1-w)(a_2-w)))U_L = sU_L$ where w is the uniform width of the gap around the plate and $U_L$ is the velocity of the piston which is equal to 2Df. Rigorously speaking, the latter value is only an approximation since the piston accelerates/decelerates near the two end points of its trajectory. However, the end points acceleration/deceleration represents less than 10% of the total motion time so it can be ignored. The factor s takes large values so the fluid velocity in the gap is much larger than the piston velocity. The system of two transient momentum equations and

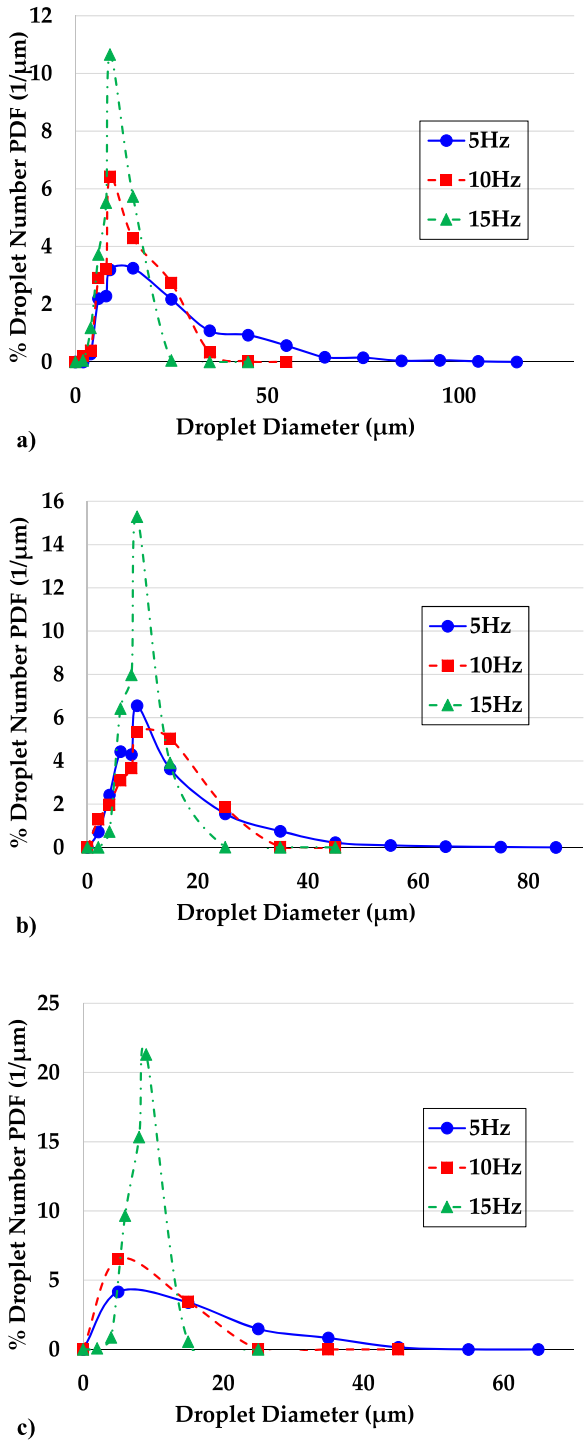


**Fig. 6.** Effect of stroke frequency f on droplet size probability density function for piston 4 and different emulsification times. a) $t_n = 0.5$ min; b) $t_n = 2$ min; c) $t_n = 10$ min.

continuity equation has to be solved with boundary conditions $u_x = 0$ on the piston wall and $u_x = U_L$ at the cell wall (the moving cartesian coordinate system is shown in Fig. 8). The exact profile of velocity at the inlet is partially known since only its average value U and the cell wall value $U_L$ have been defined. The residence time of the fluid in the gap is δ/U which is much smaller than the characteristic motion time 1/2f so pseudosteady conditions can be assumed. The final equations system is a 2-dimensional entry flow problem. This problem must be solved numerically for the complete velocity profile. However, at small lengths along the flow, two independent boundary layers are developed at the two walls. The thickness of these boundary layers at the rear of the gap is given by the relation $\lambda = (\nu\delta/U)^{0.5}$. The relation $\lambda/w < 1/2$ always holds in the present experiments so the flow in the gap can be described by two boundary layers at the walls, and the numerical solution of the full Navier-Stokes equation is not needed. Evaluation of the Reynolds number $N_{Re1}=Uw/\nu$ and $N_{Re2}= U\delta/\nu$ confirms their laminar character. The parameter s is large for most of the present experimental configurations so it is a good approximation to neglect the cell wall velocity (being an order of magnitude smaller than the velocity of fluid entering the gap). Using the Pollhausen expression [27] for the laminar boundary layer velocity profile and performing a liquid mass balance along the flow the following approximating velocity ux profile in the gap can be found.

$$u_x=(2\eta-2\eta^3+\eta^4)(1-0{\cdot}6\lambda_x/w)^{-1}U \tag{2}$$

where.

$$\eta=y/\lambda_x \text{ and } \lambda_x=(\nu x/U)^{0.5} \tag{3}$$

The fraction of the liquid having passed through the boundary layers to the total liquid volume for every single trajectory of the piston is given as

$$r = \frac{1.4\lambda/w}{1-0.6\lambda/w} \tag{4}$$

The maximum shear stress at the exit of the gap at $x = \delta$ is given as

$$G_{\max} = \frac{2U}{w(1-0.6\lambda/w)} \tag{5}$$

As a summary of the above discussion, a qualitative sketch of the flow field in the cell is shown in Fig. 9. It is noticed that the term "irrotational" refers to the primary fluid flowfield created by the motion of the piston. The secondary field contains residual vorticity remained from the previous piston oscillation single. The values of parameters r and $G_{max}$ for the present experiments appear in Table 4. These parameters are of importance for the future modeling of the breakage process.

### 4.2. Volumetric average droplet diameter

The computed characteristic average velocities of the phase separation front can be assumed to represent the buoyancy velocity of an "average" droplet size. The latter is expected to be closer to the volumetric average droplet size since optical observation of the separating front is related mainly to the volumetric fraction of the two phases. A simple idea is to use a theoretical expression for the buoyancy velocity and equate it to the measured phase separation velocity and so create an algebraic problem that must be solved for an "average" size. The expression for the buoyancy takes into account the existence and interaction of other neighboring droplets around the one examined, and the non-zero value of Reynolds number for the droplets of the present work. The combination of small droplet sizes and high surfactant concentration suggests that the liquid can be considered contaminated and so surface elasticity makes the droplet to behave as solid particle (with respect to hydrodynamic drag) [28]. The bulk viscosity of the liquid phase is not affected by the particular surfactant concentration employed here. The wall effect on the droplet motion is not accounted since for a concentrated emulsion it concerns only droplets in very small distances from the wall. The resulting buoyancy velocity $U_b$ expression is (Re number is computed using the Stokes velocity u) as [29]:

$$u = \frac{(\rho_w - \rho_{oil})g d_v^2}{18\mu} \tag{6}$$

$$U_b = u(1+3\mathrm{Re}/16)(1-\varphi)^{(1.791+0.133\mathrm{Re}^{0.456})/(0.359+0.093\mathrm{Re}^{0.456})} \tag{7}$$

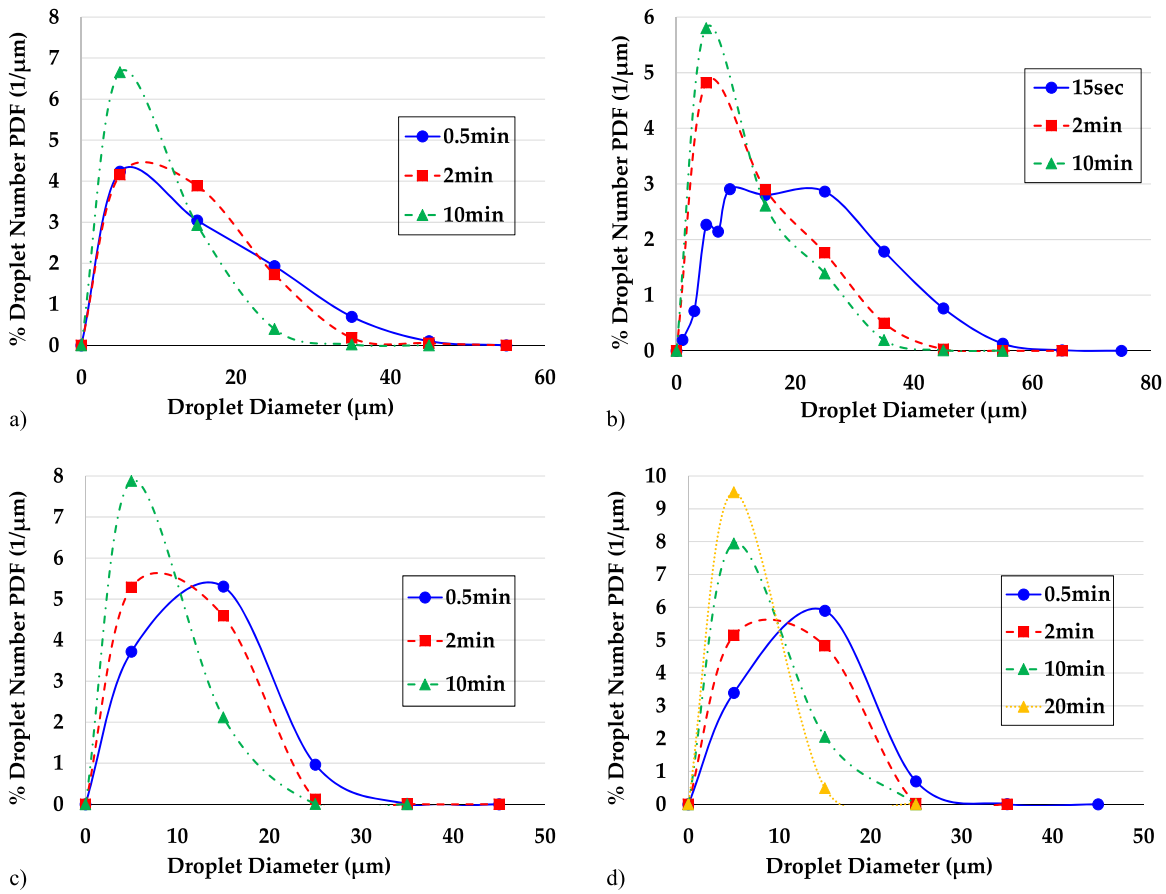


**Fig. 7.** Effect of emulsification time $t_n$ on droplet size probability density function for different pistons and stroke frequencies. a. piston 1, f = 15 Hz; b. piston 3, f = 10 Hz; c. piston 3, f = 15 Hz; d. piston 5, f = 15 Hz.

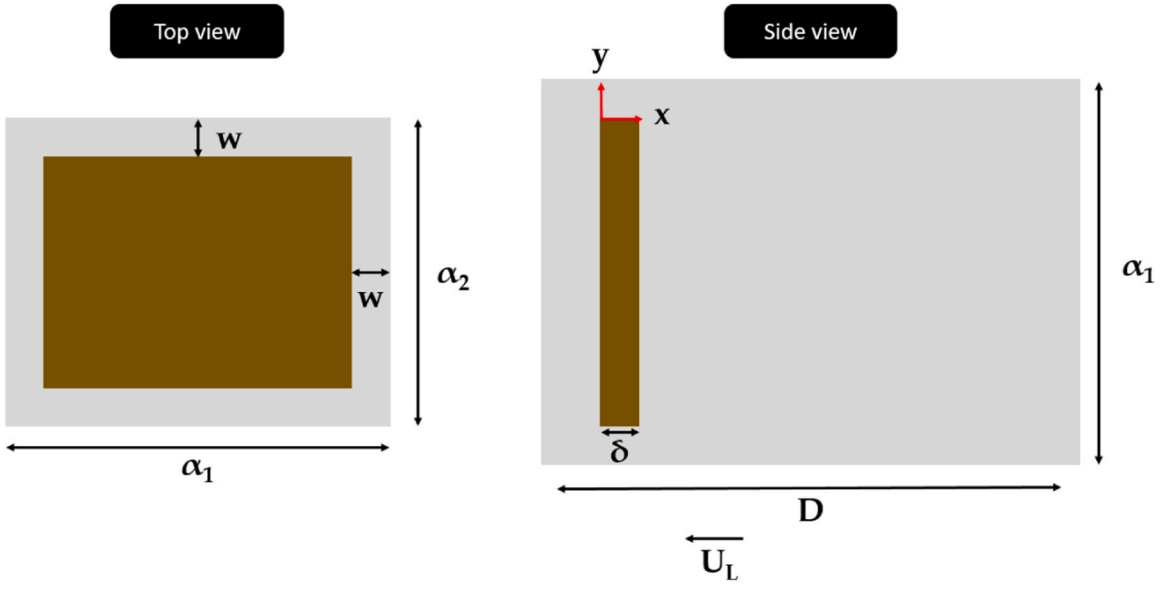


**Fig. 8.** Top and side view of cell cross sections. The dark orthogonals designate the plate of the piston.

where μ is the continuous phase (water) viscosity, $\rho_w$, $\rho_{oil}$ are the water and oil densities, respectively, g is the gravitational acceleration, φ is the oil volume fraction and $d_v$ is the "volumetric average" droplet diameter. No emulsification parameters appear in Eqs. (6, 7) since emulsification contributes to phase separation only through droplet size. The above equation is solved numerically to give $d_v$ for the measured value of $U_b$. The value of $d_v$ has been calculated for all the experimental conditions of the present work and they are presented in Fig. 10. These results will be discussed later.

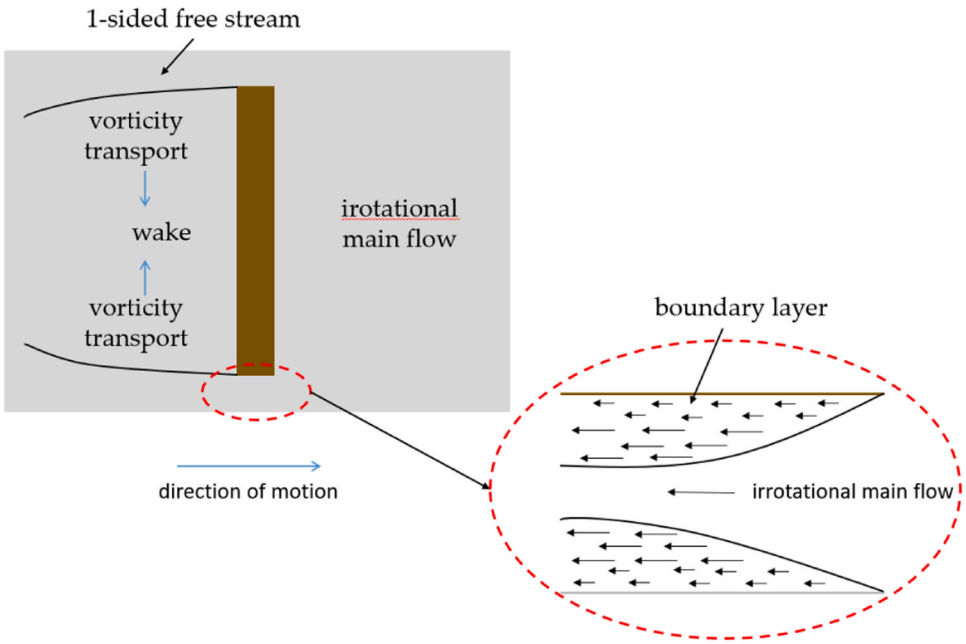


**Fig. 9.** A qualitative scetch of the flowfield in the cell.

**Table 4**
Main features of the flow field for the performed experiments.

| | f (Hz) | U (m/s) | λ (mm) | λ/w | r | $G_{max}$ (1/s) |
|---|---|---|---|---|---|---|
| Piston 1 | **5** | 0.559 | 0.0538 | 0.0815 | 0.12 | 1781 |
| | **10** | 1.118 | 0.038 | 0.0576 | 0.0836 | 3509 |
| | **15** | 1.677 | 0.031 | 0.047 | 0.0678 | 5230 |
| | **20** | 2.236 | 0.0269 | 0.0407 | 0.0585 | 6946 |
| Piston 2 | **5** | 0.903 | 0.0423 | 0.105 | 0.158 | 4822 |
| | **10** | 1.806 | 0.0299 | 0.0748 | 0.109 | 9456 |
| | **15** | 2.709 | 0.0244 | 0.0611 | 0.0888 | 14063 |
| Piston 3 | **5** | 1.427 | 0.0336 | 0.134 | 0.205 | 12427 |
| | **10** | 2.855 | 0.0238 | 0.0952 | 0.141 | 24231 |
| | **15** | 4.283 | 0.0194 | 0.0777 | 0.114 | 35947 |
| Piston 4 | **5** | 1.427 | 0.0264 | 0.105 | 0.158 | 12197 |
| | **10** | 2.855 | 0.0187 | 0.0748 | 0.109 | 23920 |
| | **15** | 4.283 | 0.0152 | 0.0611 | 0.0888 | 35574 |
| Piston 5 | **5** | 1.427 | 0.0418 | 0.167 | 0.26 | 12698 |
| | **10** | 2.855 | 0.0295 | 0.118 | 0.178 | 24592 |
| | **15** | 4.283 | 0.0241 | 0.0966 | 0.143 | 36378 |

### 4.3. Measured droplet size distribution

There are several methods to measure particle size distribution. Each of them is based on characterizing particles by a size dependent weight. In the simplest case, this weight is proportional to a power of the droplet diameter (e.g. diameter, cross section area, volume etc). Another distinction of these methods is between single particle counting (e.g. image analysis) or integral quantities over particles size distribution counting (e.g. light scattering based methods). Both categories have problems to reconstruct a very broad droplet size distribution. The problem in image processing is the huge number of droplets that must be considered as polydispersity increases [30,31] whereas for the light scattering methods the problem is the increasing ill-position of the corresponding mathematical inverse problem [32].

In the present work, the initial condition is an oil blob which breaks successively creating very broad droplet size distributions until converging to a narrower one as the breakage process proceeds. The interest here is to the evolving broad droplet size distributions. No single measurement technique can give a reliable account of the complete size distribution in this case. The idea here is to combine results from image processing with the estimation of a "volumetric average" characteristic size emerging from phase separation experiments. An additional problem, common to the image-based techniques, is that a detection limit to droplet sizes ($d_{min}$) exists. In order to become explicit and demonstrate the implications of the above discussion let us denote as F(d) the actual probability density function of droplet diameters. There is a maximum size $d_{max}$ beyond which the droplets elude (due to sampling procedure) or are too few to affect the number probability function. The image-based technique applied here essentially constructs the following probability density function g(d)

$$g(d) = \frac{F(d)}{\int_{d_{min}}^{d_{max}} F(d)dd} \text{ ford}_{min} < d < d_{max} \quad (8)$$

g(d)= 0 for other d values.

There is no way to reconstruct F(d) from g(d). However, an additional information can be extracted by considering the very approximate relation:

$$d_v = \left(\int_0^{\infty} d^3 F(d)dd\right)^{1/3} \quad (9)$$

Finally, no explicit information for F(d) in the region $d<d_{min}$ exists. Nevertheless, the quality (haze) of the background in images and the shape of g(d) close to $d_{min}$ suggests about the existence (or not) of a considerable droplet number in this region. The relation between actual droplet size distribution and measured variables appears schematically in Fig. 11. The above discussion on what is actually measured in the present work is essential in view of discussing the result of these measurements.

## 5. Discussion

In the absence of droplets coalescence, emulsification is driven by droplets breakage. The theory of breakage of fluid dispersions in a flow field has been extensively treated in literature. It appears that shear stresses (and pressure fluctuations in case of turbulent flow) are the disruptive forces whereas interfacial tension and viscosity of the (dispersed phase) droplets produce the forces opposing breakage. Interfacial elasticity typically weakens (slightly) the opposition produced by interfacial tension promoting in this way the breakage [33]. However, the main effect of surfactant is the enhancement of breakage

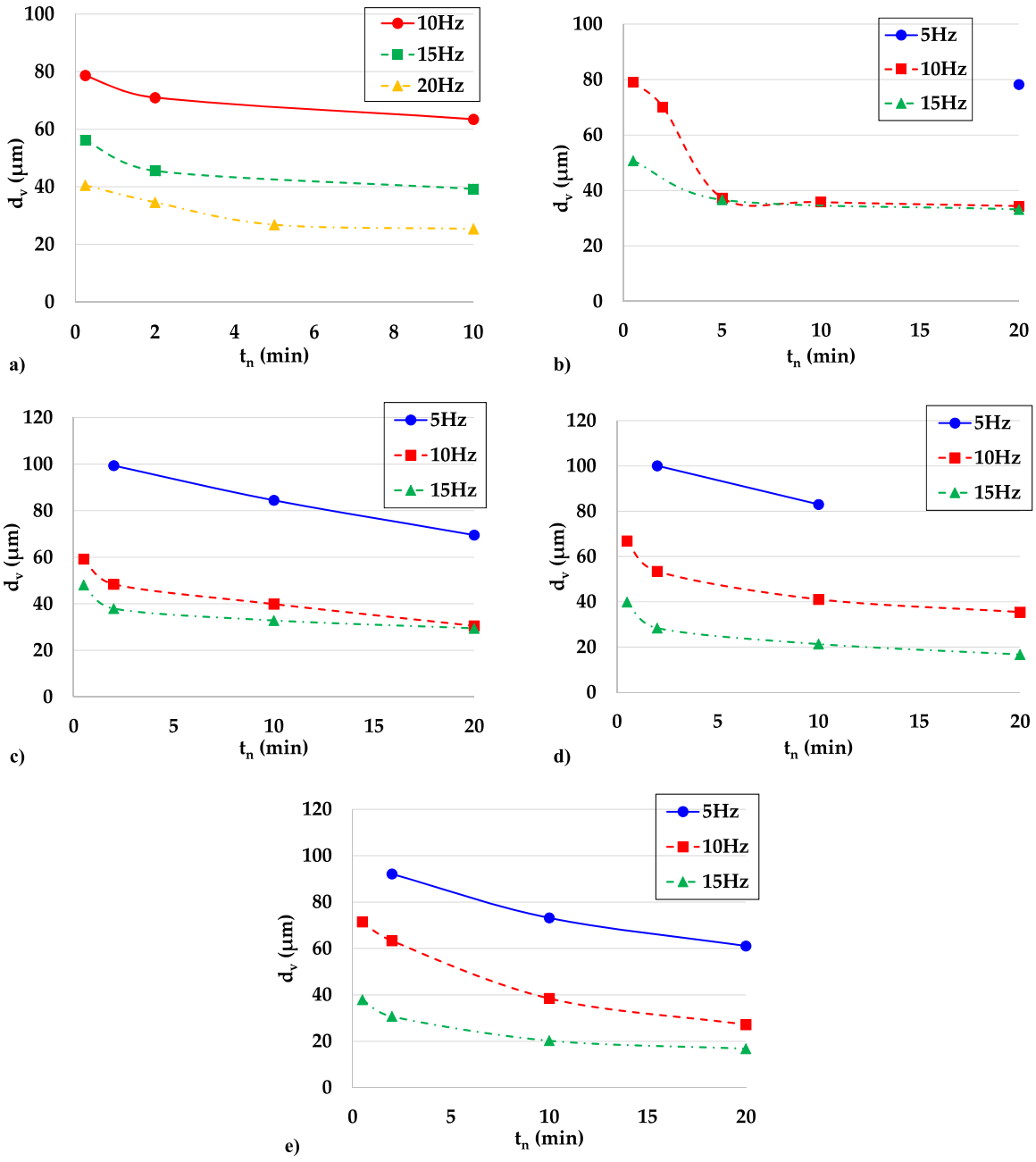


**Fig. 10.** Volumetric average droplet diameter $d_v$ versus emulsification time for different stroke frequencies. a) Piston 1; b) Piston 2; c) Piston 3; d) Piston 4; e) Piston 5.

by lowering interfacial tension. There are detailed analytical and numerical models for breakage for droplets in a steady linear flow field (shear or extensional). The mechanism of breakage in this case is well understood and a complete description can be found in literature (see for example [34]). The mode of breakage (and correspondingly the number of fragments) depends mainly on viscosity ratio (droplet to bulk viscosity) and capillary number Ca which denotes the ratio of fluid stresses to surface tension forces. For given viscosities the fragmentation rate increases as Ca increases. In case of turbulent flow, there are only a few numerical simulations for isotropic turbulence and for actual flow fields [35]. However, there is a very extensive literature on phenomenological models for breakage rate and fragments distribution based on statistical theory of isotropic turbulence. The pioneering work of Hinze [36] suggested the existence of a maximum droplet size able to survive in the flow field. Latter it was shown that this size is not really stable but denotes the frontier between two different ranges of breakage rate [37]. The turbulent breakage models consider always that two fragments appear per breakage event. The size of fragments is unequal for larger droplets and tends to equality as droplet size decreases.

The residence time of droplets in the gap is too small for breakage induced by evolving shear to occur. A more relevant to the present situation mode of breakage is the one of calming after exposure to linear laminar flow [38]. The droplet is elongated during linear flow and then two possibilities exist during the no flow period, depending on its elongation: i) If it is larger than a critical value a very fast break-up occurs. ii) If it is smaller from this critical value it recovers the initial spherical shape in the time scale of $t_c = \mu R(1 + \mu_d/\mu)/\sigma$ [39] where $\mu_d$ is the droplet viscosity, σ is the interfacial tension and R is the droplet radius. In the present device breakage occurs in a laminar boundary layer. There is no fundamental theory for this case so arguments from

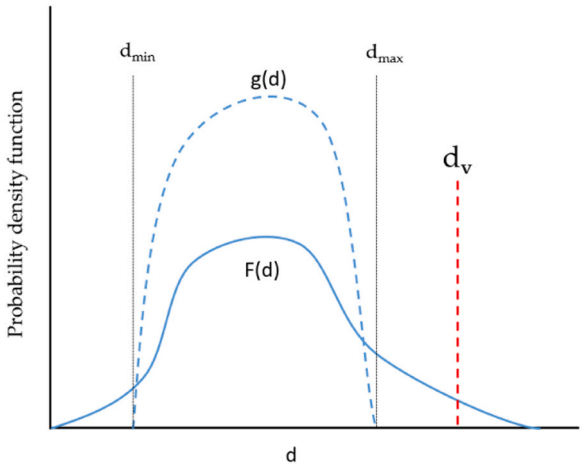


**Fig. 11.** Actual (continuous line) F(d) and measured (dashed line) g(d)+$d_v$ probability density functions of droplet sizes.

the linear flow will be used for the description of the process.

Connecting all the above information let us now try to describe what happens in the present experimental cell. Initially some kind of interfacial instability leads to withdrawing of droplets from the oil mass leading to a quite bimodal size distribution. As this process continues the two modes meets each other in the form of a very broad distribution. This initial stage is very complex to be further analyzed due to size scale of the oil blobs. The breakage mechanism for the (withdrawn from the blobs) droplets is the following: A small portion of the fluid at each stroke flows through the boundary layers created by the piston motion. The droplets in there, are elongated further from their critical size and as a result they breakup during their resting time after the passage from the gap. The relaxation time $t_c$ is much smaller than the resting time 1/(2 f) and the residence time in the boundary layer is extremely small so the above is the only viable scenario for breakage. The fact that most of the droplets pass the gap without breakage (breakage is experienced by only a random small fraction located in the boundary layer) can be confirmed by a simple counting of breakage events and passages through the gap. Let us consider a period of intense breakage e.g. Piston 2, 10 Hz, 0.5–5 min. The diameter d is reduced about 4 times during this period implying at most, i.e., by assuming binary breakage, 6 breakage events for a single droplet. During this time the droplet passes 5400 times (=4.5 *60 *20) through the gap which implies a single breakage event of the droplet per 900 passages. The number of passages for a breakage event to occur is even larger in other cases. The above picture is in accordance to video recordings through the observation window during emulsification: No breakage event in the gap is registered. An illustration demonstrating the steps of the breakage process appears in Fig. 12.

The average diameter evolution curves, Fig. 5, are quite reminiscent to those valid in turbulent breakage: The size reduction rate (slope of the curves) starts from large values and quickly drops to vanishingly small values leading to a pseudoequilibrium during which the existing droplets can no longer break. In this pseudoequilibrium state the smaller droplets are coming from a few breaking events of much larger droplets (fragments) whereas the larger droplets come from many repeated breaking events (mother droplets). One could roughly say that the two values $d_{av}$ and $d_v$ characterize the above two types of droplets.

The evolution of the mother mode size $d_v$ appearing in Fig. 10 suggests that it decreases with emulsification time and it decreases with stroke frequency, too, as expected. The same behavior appears in general to hold for $d_{av}$ in Fig. 5 except in some cases (e.g., piston 1, 5 Hz in Fig. 5**a)** where $d_{av}$ appears to increase with time or frequency. The latter is not due to experimental error but to the way of data interpretation. In the piston 1 and 5 Hz case, $d_v$ is so large that a respective curve could also not be captured in Fig. 10**a**. This means that initially the mother mode escapes optical depiction and so it is not counted in the calculation of $d_{av}$ (i.e. it includes droplets larger than $d_{max}$). As time proceeds and mother mode droplets are breaking up, their size cross the boundary of $d_{max}$ and they are progressively counted in $d_{av}$ leading to its apparent increase in time. This behavior is also the reason for increasing $d_{av}$ with increasing f observed in some cases. Most of the problematic cases are associated to very large (not measurable) values of $d_v$ confirming the above explanation. It is observed that $d_{av}$ converges faster to steady state than $d_v$. This is in accordance with the above described picture. Non-breakable fragments are leveling off in fragment mode whereas mother droplet continues to break.

The next step is to evaluate the performance of the pistons. The larger the width of the gap the smaller the possibility of a droplet to be in the boundary layer (smaller r) and the smaller the breakage performance. This is clear regarding Piston 1 which has the lowest breakage performance (check $d_{av}$ for f=15 Hz and $t_n$ =10 min) due to the large gap width. The frequency f must be increased to 20 Hz to achieve the performance of the other pistons with 15 Hz. In principle, the width of the gap increases the breakage performance by increasing the boundary layer thickness λ. However the differences in the performance of Pistons 2–5 are marginal. Let us consider the most efficient breakage conditions of $t_n$ = 20 min and f= 15 Hz. The most efficient Piston under these conditions is the number 5 (considering both $d_{av}$ and $d_v$) as expected since it has minimum gap

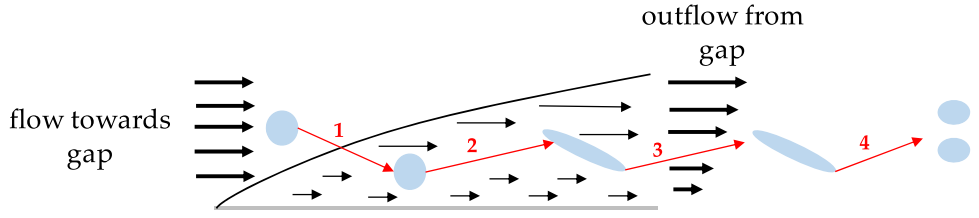


**Fig. 12.** Steps of the proposed breakage process: (1) entrainment of droplet in the boundary layer (2) droplet elongation beyond their critical size (3) exit from boundary layer (4) breakup during resting period.

width and maximum gap height. However all pistons 2–5 are very efficient under these conditions (the actual value of d would be even smaller in the absence of detection limit $d_{min}$). It is noted that for pistons 2–5, for $f \geq 10$ Hz and $t_n \geq 5$ min the haziness in the images indicates the existence of droplets with size smaller than $d_{min}$. If in the selection of the optimum piston performance the emulsification time and energy consumption is included then the optimum choice is Piston 2 with $f = 10$ Hz and $t_n = 10$ min. In this case the performance is somewhat worse but there is a large economy of time and energy. The above discussion refers of course to the particular system examined but similar assessment is expected for other systems in case of larger surfactant concentration (i.e. non coalescing system) and smaller oil volume fraction.

## 6. Conclusions

The efficiency of a new emulsification device capable of handling liquid volumes of just few milliliters is examined with respect to geometric features of its main element (oscillating piston with a plate attached to its tip). The evolution of droplet sizes is presented for a specific system dominated by breakage. The transient droplet size distributions are very broad so two different methods are employed to cover their size range. A theoretical analysis suggests that the droplets are elongated, beyond their critical size, inside the boundary layers developed in the gap between the plate and cell walls, and then they break in the domain behind the gap. Only a small fraction of droplets undergoes breakage during their passage from the gap. Optical observations in the cell during emulsification using a high speed camera, do not reveal any breakup effect in accordance to the suggested breakage mechanism. A boundary layer breakage model has to be developed in order to interpret better the results of the present work. It appears that from the examined five piston geometries only the one with the largest gap width exhibits an inferior performance. The other 4 pistons give comparable results and they all exhibit high performance. The one with the highest gap width and height appears to produce slightly smaller droplets. Conclusively, the new device with a thin gap of 0.25 mm is adequate to produce an emulsion under small volume restriction.

## CRediT authorship contribution statement

**Angeliki P. Chondrou:** Conceptualization, Data Curation, Methodology, Writing - original draft preparation. **Thodoris D. Karapantsios:** Conceptualization, Funding acquisition, Project adiministration, Writing - review & editing. **Margaritis Kostoglou:** Conceptualization, Data curation, Formal analysis, Validation, Supervision, Writing - original draft preparation, Writing - review & editing.

## Declaration of Competing Interest

The authors declare that they have no known competing financial interests or personal relationships that could have appeared to influence the work reported in this paper.

## Acknowledgements

This research was supported by the European Space Agency (ESA) MAP PROJECT “Emulsion Dynamics and Droplet Interfaces (EDDI)” – Contract No.: 4000128643/19/NL/PG.

## References

[1] C.D. Ampatzidis, E.M. Varka, T.D. Karapantsios, Interfacial activity of amino acid-based glycerol ether surfactants and their performance in stabilizing O/W cosmetic emulsions, Colloids Surf. A: Physicochem. Eng. Asp. 460 (2014) 176–183.
[2] J.S. Hong, J. Bergfreund, P. Fischer, Complex emulsion stabilization behavior of clay particles and surfactants based on an interfacial rheological study, Colloids Surf. A: Physicochem. Eng. Asp. 602 (2020), 125121.
[3] L.L. Schramm, Emulsions, Foams and Suspensions, Fundamentals and Applications, Wiley-VCH Verlag GmbH & Co, KGaA: Weinheim, Germany, 2005.
[4] T.F. Tadros, Emulsions Formation and Stability, Wiley-VCH, Weinheim, 2013.
[5] R.J. Farn, Chemistry and Technology of Surfactants, Blackwell Publishing Ltd, 2006.
[6] V. Lorusso, D. Orsi, F. Salerni, L. Liggieri, F. Ravera, R. McMillin, J. Ferri, L. Christofolini, Recent developments in emulsion characterization: diffusing wave spectroscopy beyond average values, Adv. Colloid Interface Sci. 288 (2021), 102341.
[7] M.J. Rosen, Surfactants and Interfacial Phenomena, third ed., John Wiley & Sons Inc, New Jersey, 2004.
[8] J.M. Leiva, E. Geffroy, Evolution of the size distribution of an emulsion under a simple shear flow, Fluids 3 (2018) 46.
[9] F. Mirshekari, L. Pakzad, P. Fatehi, An investigation on the stability of the hazelnut oil-water emulsion, J. Dispers. Sci. Technol. 41 (6) (2020) 929–940.
[10] F. Goodarzi, S. Zendehboudi, A comprehensive review on emulsions and emulsion stability in chemical and energy industries, Can. J. Chem. Eng. 97 (2019) 281–309.
[11] E.M. Varka, T.D. Karapantsios, Global versus local dynamics during destabilization of eco-friendly cosmetic emulsions, Colloids Surf. A Physicochem. Eng. Asp. 391 (1–3) (2011) 195–200.
[12] D. Orsi, F. Salerni, E. Macaluso, E. Santini, F. Ravera, L. Liggieri, L. Christofolini, Diffusing wave spectroscopy for investigating emulsions: I. Instrumental aspects, Colloids Surf. A: Physicochem. Eng. Asp. 580 (2019), 123574.
[13] M.C. Vlachou, K.A. Zacharias, M. Kostoglou, T.D. Karapantsios, Droplet size distributions derived from evolution of oil fraction during phase separation of oil-in-water emulsions tracked by electrical impedance spectroscopy, Colloids Surf. A: Physicochem. Eng. Asp. 586 (2020), 124292.
[14] A. Belkadi, D. Tarlet, A. Montillet, J. Bellettre, P. Massoli, Study of two impinging flow microsystems arranged in series. Application to emulsified biofuel production, Fuel 170 (2016) 185–196.
[15] M. Ashar, D. Arlov, F. Carlsson, F. Innings, R. Andersson, Single droplet breakup in a rotor-stator mixer, Chem. Eng. Sci. 181 (2018) 186–198.
[16] D. Gazolu-Rusanova, I. Lesov, S. Tcholakova, N. Denkov, B. Ahtchi, Food grade nanoemulsions preparation by rotor-stator homogenization, Food Hydrocoll. 102 (2020), 105579.
[17] M.V. Kempin, M. Kraume, A. Drews, W/O pickering emulsion preparation using a batch rotor-stator mixer – Influence on rheology, drop size distribution and filtration behavior, J. Colloid Interface Sci. 573 (2020) 135–149.
[18] S.M. Niknam, I. Escudero, J.M. Benito, Formulation and preparation of water-in-oil-in-water emulsions loaded with a phenolic-rich inner aqueous phase by application of high energy emulsification methods, Foods 9 (2020) 1411.
[19] S. Akbari, A. Hamid, Emulsion types, stability mechanisms and rheology: a review, Int. J. Innov. Res. Sci. Stud. 1 (1) (2018) 14–21.
[20] A.P. Chondrou, S.P. Evgenidis, M. Kostoglou, T.D. Karapantsios, An innovative miniature pulsating emulsification device: flow characterization and measurement of emulsion stability, Colloids Interfaces 4 (2020) 7.
[21] Y. Ji, J. Bellettre, A. Montillet, P. Massoli, Fast oil-in-water emulsification in microchannel using head-on impinging configuration: effect of swirl motion, Int. J. Multiph. Flow 131 (2020), 103402.
[22] A. Belkadi, D. Tarlet, A. Montillet, J. Bellettre, P. Massoli, Water-in-oil emulsification in a microfluidic impinging flow at high capillary numbers, Int. J. Multiph. Flow 78 (2015) 11–23.
[23] S. Llamas, E. Santini, L. Liggieri, F. Salerni, D. Orsi, L. Christofolini, F. Ravera, Adsorption of sodium dodecyl sulfate at water-dodecane interface in relation to the oil in water emulsion properties, Am. Chem. Soc. 34 (2018) 5978–5989.
[24] L. Marchitto, R. Calabria, C. Tornatore, J. Bellettre, P. Massoli, A. Montillet, G. Valentino, Optical investigations in a CI engine fueled with water in diesel emulsion produced through microchannels, Exp. Therm. Fluid Sci. 95 (2018) 96–103.
[25] X. Zabulis, M. Papara, A. Chatziargyriou, T.D. Karapantsios, Detection of densely dispersed spherical bubbles in digital images based on a template matching technique. Application to wet foams, Colloids Surf. A Physicochem. Eng. Asp. 309 (1–3) (2007) 96–106.
[26] C. Pozrikidis, Introduction to Theoretical and Computational Fluid Dynamics, Oxford University Press, New York, 1997.
[27] W.M. Deen, Analysis of Transport Phenomena, Oxford University Press, New York, 1998.
[28] A.V. Nguyen, H.J. Schulze, Colloidal Science of Flotation, Marcel Dekker, New York, 2004.
[29] M. Kostoglou, E.M. Varka, E.P. Kalogianni, T.D. Karapantsios, Evolution of volume fractions and droplet sizes by analysis of electrical conductance curves during destabilization of oil-in-water emulsions, J. Colloid Interface Sci. 349 (2010) 408–416.
[30] S. Caserta, M. Simeone, S. Guido, Evolution of drop size distribution of polymer blends under shear flow by optical sectioning, Rheol. Acta 43 (2004) 491–501.
[31] S. Caserta, M. Simeone, S. Guido, A parameter investigation of shear-induced coalescence in semidilute PIB-PDMS polymer blends: effects of shear rate, shear stress volume fraction and viscosity, Rheol. Acta 45 (2006) 505–512.

[32] G.E. Elicabe, L.H. Garcia Rubio, Latex particle size distribution from turbidimetry using inversion techniques, J. Colloid Interface Sci. 129 (1989) 192–200.
[33] M.J.J. Janssen, A. Boon, M.W.G. Agterof, Droplet break-up in simple shear flow in the presence of emulsifiers, Colloids Surf. A: Physicochem. Eng. Asp. 91 (1994) 141–148.
[34] F. Risso, The mechanisms of deformation and breakup of drops and bubbles, Multiph. Sci. Technol. 12 (2000) 1–50.
[35] R. Andersson, A. Helmi, Computational fluid dynamics simulation of fluid particle fragmentation in turbulent flows, Appl. Math. Model. 38 (2014) 4186–4196.
[36] J.O. Hinze, Fundamentals of the hydrodynamic mechanics of splitting in dispersion processes, AIChE J. 1 (1955) 289–295.
[37] M. Kostoglou, A.J. Karabelas, Towards a unified framework for the derivation of breakage functions based on the statistical theory of turbulence, Chem. Eng. Sci. 60 (2005) 6584–6595.
[38] H.A. Stone, B.J. Bentley, L.G. Leal, An experimental study of transient effects in the breakup of viscous drops, J. Fluid Mech. 173 (1986) 131–158.
[39] L.G. Leal, Advanced Transport Phenomena: Fluid Mechanics and Convective Transport Processes, Cambridge University Press, Cambridge, 2007.